On Crop Canopy Scattering for Integrated mmWave Sensing and Communication in Agricultural Fields

Shuai Nie

School of Computing
University of Nebraska-Lincoln
Lincoln, NE, USA
shuainie@unl.edu

Yufeng Ge

Biological Systems Engineering University of Nebraska-Lincoln Lincoln, NE, USA yge2@unl.edu Mehmet C. Vuran
School of Computing
University of Nebraska-Lincoln
Lincoln, NE, USA
mcv@unl.edu

Abstract-Millimeter-wave (mmWave) spectrum offers wide bandwidth resources that are promising to realize highthroughput wireless communications in agricultural fields. Due to the relatively small wavelength at this frequency band, mmWave signals tend to be scattered when the wireless link is established above the crop canopy. However, little is known about the scattering effect caused by crop canopy at mmWave. In this work, the scattering loss in the mmWave spectrum is quantified for different crop canopy states that are represented by the leaf area index. In particular, an approach based on a Rayleigh roughness criterion is utilized, coupled with canopy height statistics, to calculate the scattering loss. The results of the model agree well with empirical data collected from agricultural field experiments conducted in Summer 2021. The results demonstrate that as the leaf area index decreases with crop maturity, the scattering loss also decreases. This is the first work that illustrates the feasibility of using the mmWave communication links to perform sensing on the leaf area index, which is a critical metric in estimating crop conditions.

Îndex Terms—Scattering, wireless agricultural networks, millimeter-wave communications, leaf area index, field experiments.

I. INTRODUCTION

Wideband wireless communications are crucial in enabling high-throughput networks globally [1]. In recent years, numerous solutions and applications have been developed to explore frequency spectra that offer wide bandwidth resources, leading to high spectral efficiency. These include millimeter-wave (mmWave) beamforming [2] and ultra-massive multiple-input-multiple-output (MIMO) communications [3]. While these solutions primarily target densely populated areas, such as dense urban environments and indoor offices, there is a need to explore emerging scenarios for rural broadband. Often overlooked, these scenarios include agricultural networks, where the increasing demand for precision agriculture calls not only for agricultural Internet of Things (Ag-IoT) [4], [5] but also wideband high-throughput communications and the novel sensing modalities that come within.

One critical application in precision agriculture is highthroughput and high-resolution crop phenotyping. Crop phenotyping employs images to characterize the physiological and metabolic mechanisms of plant development [6]. This

This work is partially supported by the National Science Foundation under grants 2030272 and 2212050.

method relies on high-resolution images to capture important structural and biological traits for health monitoring and yield prediction, among other purposes [7]. The size of data captured using different imaging technologies can range from a few megabytes to several gigabytes, depending on factors such as image resolution, plant size, and the complexity of the phenotyping system [8]. However, current wireless technologies used in agricultural farms, such as long-range wireless area networks (LoRaWAN), fail to satisfy the transmission requirements for plant phenotyping data. To this end, in this paper, we explore the enabling agricultural sensing and communication capabilities of the mmWave spectrum to help bridge the digital divide in high-throughput real-time wireless links for agricultural operations.

Using mmWave signals in precision agriculture sensing and communication faces several challenges. Due to their relatively small wavelength, mmWave signals are prone to scattering when encountering rough surfaces. Recently, the diffuse scattering effects of mmWave signals have been extensively studied in various materials, such as glass, dressed stone walls, soil, and tree foliage [9]-[13]. However, capturing scattering caused by crop canopies has received little attention so far. Our recent experimental results [14], [15] demonstrate that the crop canopy forms a new "ground" that induces multipath effects. Due to the randomness of leaf distribution, the crop canopy can be considered a rough surface that may cause diffuse scattering of mmWave signals. As shown in Fig. 1, when electromagnetic waves encounter the corn canopy, leaves absorb a part of the incident energy, while some of the energy is scattered back into the air in different directions. The theoretical underpinnings of the crop canopy scattering effect on mmWave signals are not well understood, which may lead to novel agricultural sensing and communication capabilities.

In this work, we model the crop canopy scattering effects at 60 GHz. We analyze the scattering loss at different growth stages of corn crops using the Rayleigh roughness criterion approach coupled with crop-related parameters. The models are validated using publicly available datasets collected through our field experiments [16]. The specific technical contributions of this work are as follows:

• We characterize the scattering effect caused by the random distribution of corn leaves using an approach based

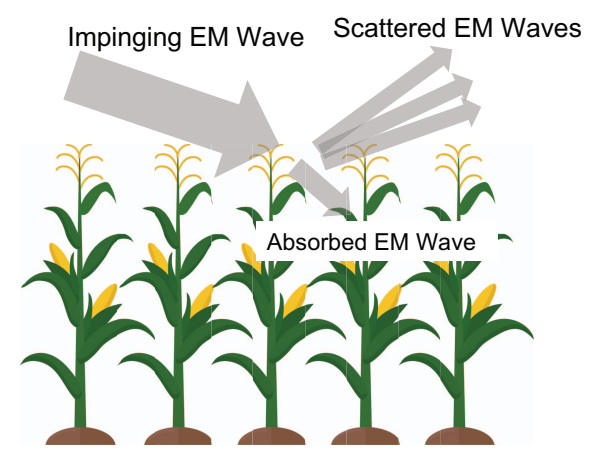


Fig. 1: Crop Canopy Scattering: Impinging electromagnetic waves are partially scattered and partially absorbed by crop canopy.

on the Rayleigh roughness criterion and coupled with canopy height statistics to calculate the scattering loss at different growth stages.

- In the Rayleigh roughness criterion model, we introduce the parameter of fractional vegetation cover to quantify the surface roughness of crop canopies.
- We analyze the scattering loss based on empirical measurements and compare it with simulation results to investigate the correlation between leaf area index and scattering effect at different crop conditions.
- Based on the calculated and measured scattering loss under various crop conditions, we explore the feasibility of using mmWave communication links for sensing the leaf area index.

By addressing the scattering effects caused by crop canopies, this research aims to advance the understanding of mmWave communication challenges in precision agriculture and pave the way for integrated mmWave sensing and communication applications in this area.

The rest of this paper is organized as follows. The related work is discussed in Section II. Background on the geometric model of crop canopy is presented in Section III. The scattering model is discussed in Section IV. The sensing of leaf area index based on communication links is described in Section V. The related field measurements and data are described in Section VI, based on which the model is validated in Section VIII. Finally, the paper is concluded in Section VIII.

II. RELATED WORK

At mmWave bands, several empirical models are built based on measurements to characterize diffuse scattering as a function of the angle of incidence and roughness of the material. For example, in [9], the 60 GHz diffuse scattering on different building materials is characterized with respect to varying distances from the surface, angles of incidence using a 2 GHz-bandwidth channel sounder. They observe high depolarization of incident signals caused by diffuse scattering.

In [10], two scattering models are derived based on radar cross-section and directive scattering theory. The forward and backscattering losses are quantified through simulations and experiments at different frequencies (from 1 GHz to 1 THz). As a promising frequency spectrum to provide ultra-wideband communication potential, measurements at 100–400 GHz are conducted in [11] to study the correlation between scattering patterns and material roughness. A numerical solution based on the finite-difference time-domain method in [12] provides an alternative to yield accurate diffuse scattering patterns of different surface roughness profiles.

In the direction of remote sensing on agricultural fields, the incidence angle will affect the estimation of crop parameters. In [13], a polarimeter at 35 GHz acting in a bistatic mode is used to characterize the scattering coefficient of two types of tree foliage and sand surfaces. Their results show that the Fresnel reflectivity of sand varies with the angle of incidence. Another important observation drawn from the bistatic scattering experiments of tree foliage is that a wideband system (with a 2-GHz bandwidth) with frequency averaging reduces the received signal's variability caused by phase interference. To the best of our knowledge, no existing work has been done to study the scattering effects of crop canopies at the mmWave spectrum. Bridging this research gap will provide helpful insights when designing wideband wireless communication solutions for precision agriculture.

III. BACKGROUND: GEOMETRIC MODEL OF CROP CANOPY

A geometrical description of crop canopy is necessary to study the scattering effects of crop canopy on electromagnetic waves. For a single corn leaf, its shape is usually described as linear or linear-lanceolate with a width (denoted as w) and length (denoted as l) [17], which can be approximated as a rectangle. In the field, the geometry of crop canopy relies not only on the individual leaf shape but also on (1) how the leaves are oriented in the angular domain and (2) how they may be distributed and/or overlapped in the spatial domain. Thus, models of leaf angle distribution and fractional vegetation cover are needed, as described next.

A. Leaf Angle Distribution

Each leaf has a unique angle, the *leaf inclination angle*, and its value can change with different plant species, genotypes, growth stages, and wind [18]. The distribution of this angle captures the probability of leaf inclination angles taking specific or a set of values in the spatial domain. The leaf angle distribution (LAD) is an important factor in estimating the canopy's spectral reflectance (or albedo) and transmission properties that are critical for light interception and photosynthesis [19]. In particular, the leaf inclination angle is defined as the angle between the zenith direction and the normal direction of the leaf, as illustrated in Fig. 2. In our study, the factor of LAD can help us distinguish different types of crop canopies. For example, for corn leaves, the spherical LAD is a widely used model, where the distribution function can be expressed

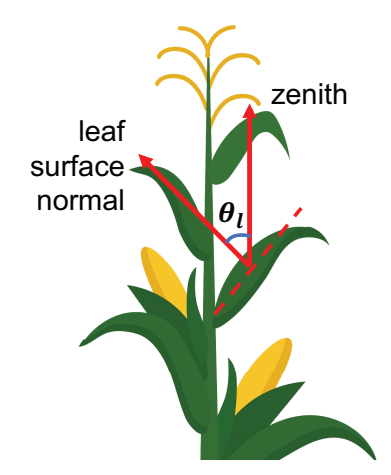


Fig. 2: Illustration of leaf inclination angle.

as $f(\theta_l) = \sin(\theta_l)$, where θ_l is the leaf inclination angle in radian [20]. It is shown that the spherical distribution is independent of viewing angles [21], which makes it suitable for incidence with low grazing angles. The assumption of spherical LAD is essential for understanding the gap fraction in vegetation or fractional vegetation cover.

B. Fractional Vegetation Cover of Crop Canopy

When electromagnetic (EM) waves impinge on a medium or a material, the material will absorb a portion of the energy. Due to the principle of energy conservation, there is also partial energy reflected or scattered from the canopy, as illustrated in Fig. 1. Since canopies are not fully continuous objects (i.e., different from glass or metal, which is a continuous piece of material) but with gaps between leaves, and the leaves have different inclinations (Sec. III-A), the fractional vegetation cover is often used to describe the percentage of space covered by a canopy, which is expressed as [22]

$$g(\theta_i) = 1 - \exp\left(\frac{-0.5F}{\cos \theta_i}\right),\tag{1}$$

where F is the leaf area index (further discussed in Sec. III-C) and θ_i is the angle of incidence, which is independent of θ_l . Notably, this model only applies to spherically distributed leaves as discussed in Sec. III-A.

C. Leaf Area Index

The leaf area index (LAI) is the single most important parameter in characterizing the productivity of both natural and agricultural ecosystems and is intensively studied in optical remote sensing [23]. LAI is defined as the ratio between the one-sided green leaf area and unit ground surface area [24]. The value of LAI ranges from 0 (i.e., bare ground) to 6–7 (i.e., peak growing season) for corn and soybean [15]. LAI reflects the *concentration* of biomass, water, and other biochemical substance (ions, electrolytes) on a unit ground area that makes it analogous to the dielectric properties of a material.

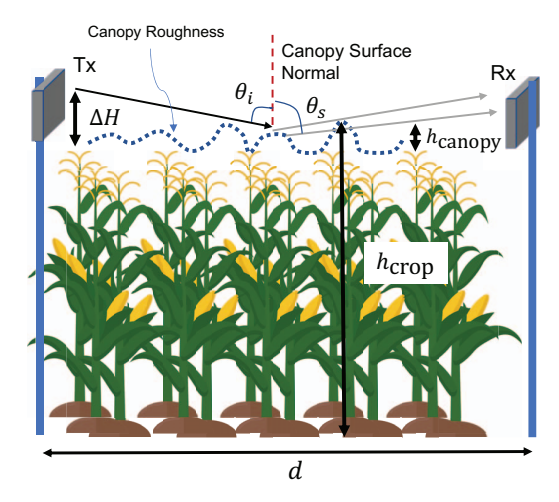


Fig. 3: Illustration of canopy scattering model. The Tx and Rx are separated by a distance d with their height above the canopy by ΔH . In addition to the LoS propagation, the scattered paths in grey are due to partial EM wave impinging on (with an incident angle θ_i) the rough canopy surface (abstracted in the dashed blue curve) with a height h_{canopy} . Including the canopy portion, each plant has a total height of h_{crop} .

D. Stratified Layers of Crop Canopy

Tree canopies in a rain forest are defined with stratified layers in the vertical direction (from bottom to top) as forest floor, understory layer, canopy layer, and emergent layer [25]. To help describe and analyze the geometric model of crops in a similar way, we define the portion of individual crops growing above the average height of the canopy as the emergent layer, as illustrated in Fig. 4.

IV. SCATTERING MODEL OF CROP CANOPY

In this section, we study the scattering effect of crop canopies at the mmWave spectrum, which is the main contribution of this paper. In particular, we analyze the scattering loss under different crop conditions. The scattering loss is computed as the difference between the received power of the path scattered from the canopy along the direction of specular reflection (i.e., toward the receiver) and that of a theoretical specular reflection path if the medium is lossless. Although both Tx and Rx are in boresight, due to the very narrow beamwidth of the antenna array, the beams that are scattered off the corn canopy can still be distinguished during beam sweeping.

As shown in Fig. 3, crop canopies are composed of individual leaves with different inclination angles. In order to draw a comparison with our field experiment data, we only consider paths scattered in the general direction following the specular reflection ($\theta_s = \theta_i$) that can be captured by the receiver. The scattering loss is determined by the scattering loss factor, which depends on the permittivity of the medium, which, in our study, is the permittivity of the canopy. Since canopies are composed of leaves, the permittivity of canopies can be approximated as that of a single leaf. The complex-

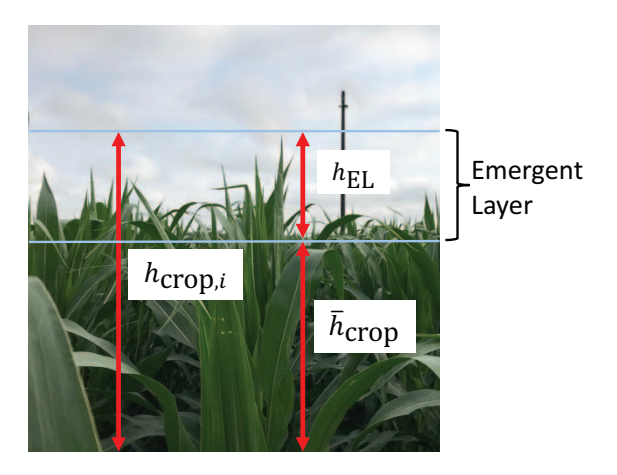


Fig. 4: Relationship between crop height, average crop height, and height of the emergent layer of the canopy.

valued permittivity, ϵ , in the spectral range of 1–100 GHz with salinity level around 1% can be expressed as [26]:

$$\epsilon = 0.522(1 - 1.32m_d)\epsilon_{SW} + 0.51 + 3.84m_d,$$
 (2)

where m_d is the dry-matter fraction and is calculated as

$$m_d = 1 - M_q = 1 - \theta_v \times \rho_w,\tag{3}$$

 θ_v is the volumetric leaf-water content, ρ_w is the water's density (near $1~{\rm g/cm^3}$), and M_g is the gravimetric water content. In (2), the permittivity of saline water is $\epsilon_{\rm SW}=\epsilon_{\rm SW}'+i\epsilon_{\rm SW}''$, which is empirically derived from [27, §4.2]. The imaginary part of the permittivity (i.e., $0.522(1-1.32m_d)\epsilon_{\rm SW}''$) determines the loss of electromagnetic energy due to absorption. Note that this model only holds when $0.1 \leq m_d \leq 0.5$. Therefore, when the dry-matter fraction exceeds the threshold of 0.5, or the volumetric leaf-water content, θ_v , drops below 0.5, the model may lose its accuracy.

In [28], a resistive sheet model is used to describe a leaf as a thin-layer dielectric material with its resistance calculated as

$$R = \frac{iZ_0}{k\tau(\epsilon - 1)},\tag{4}$$

where $Z_0=377~\Omega$ is the free space impedance, $k=2\pi/\lambda$ is the wavenumber with wavelength λ , τ is the leaf's thickness, and ϵ is the permittivity in (2). The reflection coefficient, Γ_E , of the electric field is expressed as [28]

$$\Gamma_E = \left(1 + \frac{2R}{Z_0} \cos \theta_i\right)^{-1}.\tag{5}$$

The angle of incidence on the canopy surface is θ_i and can be expressed as

$$\theta_i = \arctan\left(\frac{d}{2\Delta H}\right),$$
(6)

where d denotes the distance between the Tx and Rx, and ΔH is the difference in height between the transceiver and canopy, as shown in Fig. 3.

To study the diffuse scattering of microwave frequencies up to the THz band, the Rayleigh roughness criterion model is widely used, which is based on the height of the surface and the correlation length [11]. Therefore, this approach can be used under the condition that the dry-matter fraction, m_d , exceeds the suitable range. The Rayleigh roughness criterion is used to determine whether the surface is considered smooth or rough which allows impinging EM waves to be reflected in a specular direction or scattered in different directions [29]. More specifically, if the phase difference between two reflected paths is less than $\pi/2$ radians, then the surface is considered smooth; otherwise, the surface is deemed rough. This can be translated to the random height of the emergent layer $h_{\rm EL}$, which we define as the height of an arbitrary i-th crop $h_{\rm crop, i}$ subtracting the average crop height $\bar{h}_{\rm crop}$ (each plant has a unique height even at the same growth stage), as shown in Fig. 4. If the height satisfies the condition of $h_{\rm EL}$ > $\lambda/(8\cos\theta_i)$, the surface is considered rough [29]. At 60 GHz, when the angle of incidence is large, for example, at 75°, the canopy is considered rough if its height exceeds 2.4 mm, which is always satisfied among corn crop canopies [30].

For conventional types of surfaces, the roughness is determined by the RMS height [10]. However, for crop canopies, due to their unique geometric features, we introduce the fractional vegetation cover (discussed in Sec. III-B) to jointly describe the roughness of the canopy. Therefore, the roughness of the surface should consider the height variation with respect to the average height of the emergent layer of the canopy. The RMS height is commonly used to describe the variation in surface roughness [31], which, when fitting into the condition of emergent layer height, is expressed as

$$h_{\rm rms} = \sqrt{h_{\rm EL}^2 - \left(\bar{h}_{\rm EL}\right)^2},\tag{7}$$

where $h_{\rm EL}$ is the height of the emergent layer and $\bar{h}_{\rm EL}$ is its average value. We assume a Gaussian distribution for $h_{\rm EL}$ [32]. The variance of this Gaussian distribution, denoted by σ_G , would be dependent on the fractional vegetation cover. The average emergent layer height will depend on the LAD, which is $\bar{h}_{\rm EL} = \bar{l} \int_0^{\pi/2} \theta_l \sin\theta_l d\theta_l = \bar{l}$ and is the average length of a leaf. The probability density function of this Gaussian-distributed emergent layer height can be further expressed as

$$p(h_{\rm EL}) = \frac{g(\theta_i)}{\sqrt{2\pi}\sigma_G} \exp\left(\frac{-h_{\rm EL}^2 g^2(\theta_i)}{2\sigma_G^2}\right). \tag{8}$$

In this way, the observation angle, variation of the canopy's emergent layer, and roughness of the surface are coupled. The scattering loss factor is calculated as [10]:

$$\rho_s = \exp\left[-8\left(\frac{\pi h_{\rm rms}\cos\theta_i}{\lambda}\right)^2\right] J_0\left(\frac{8\pi h_{\rm rms}\cos\theta_i}{\lambda}\right), \quad (9)$$

where J_0 is the zeroth order Bessel function of the first kind. The scattering coefficient can be calculated as $\Gamma_s = \rho_s \Gamma_E$ where Γ_E is the reflection coefficient in the specular reflection

condition in (5) [11]. The power scattered off the canopy toward the direction of Rx is then expressed as

$$P_{\rm s} = \Gamma_{\rm s} P_{\rm i} = \rho_{\rm s} \Gamma_{\rm E} P_{\rm i},\tag{10}$$

where P_i is the incidence power. Therefore, we can estimate the scattered power from known incidence power and canopyrelated parameters.

V. LEAF AREA INDEX SENSING

Wireless sensor networks have been widely explored and deployed in agricultural fields as an integral part of Ag-IoT for precision agriculture [4], [5]. These networks, along with other sensing instruments, play an important role in measuring various parameters related to plant and soil conditions, yield prediction, and weather conditions. However, existing solutions often consist of standalone systems designed solely for a single sensing modality, increasing the cost of field systems. To address cost constraints and improve efficiency, there is a growing interest in integrated sensing and communication (ISAC) techniques, which enable sensing capabilities using communication signals [33]. Exploring the potential of mmWave communication links with directional beams for field-pertinent sensing is a promising approach for advanced and low-cost agricultural sensing.

One of the benefits of leveraging beam sweeping for agricultural sensing is the ability to provide high spatial granularity while maintaining communication spectral efficiency. The directional beam acts as a probe, capturing channel characteristics and embedding them in the received signals. The channel statistics can be inferred by analyzing these signals, thereby gaining insights into the physical phenomena that shape the channel (e.g., leaf structures). Since directional communication systems require frequent beam steering for beam-pair alignment and channel estimation, these signals can be utilized for agricultural sensing with minimum spectral overhead. In addition to these advantages, ISAC has the unique capability to operate in darkness, eliminating the need for ambient light required by most optical remote sensing or camera-based techniques that utilize measured reflected or backscattered signals and images for environment sensing. For example, the field phenotyping facility at UNL currently uses a camera-based technique (the Spidercam) to analyze the photosynthesis process based on calculated reflectance from image capture [23]. Since this field is also utilized as our experiment site (discussed in Sec. VI), researchers are expected to take advantage of wireless agricultural networks at mmWave bands to perform sensing in the near future.

As discussed in Sections III-IV, the leaf water content and the permittivity of crop canopies affect the leaf area index. The same factors also change the scattering behavior of mmWave signals, creating an inference path between mmWave signal behaviors and crop leaf area index. More specifically, the fractional vegetation cover, coupled with scattering loss, allows for the deduction of the leaf area index from measured received signal characteristics. This integration of communication links

TABLE I: Channel Sounder Parameters [34]

Parameter	Value
Center frequency	60.48 GHz
Bandwidth	$2.16~\mathrm{GHz}$
Antenna array size	36×8
EIRP of Tx	36 dBm
3-dB beamwidth (azimuth)	2.8°
3-dB beamwidth (elevation)	12°
Beam sweeping step (Tx & Rx)	2.8°
Sweeping range (azimuth)	±45°

for sensing functionality paves the way for new possibilities for accurately estimating key agricultural parameters.

Next, we discuss recent mmWave field experiments and evaluate the scattering model as an initial step toward this goal. We analyze mmWave signals and investigate the correlation between leaf water content, scattering behavior, and the leaf area index. This analysis will lead to advanced agricultural sensing techniques for precision agriculture, facilitating improved crop management and decision-making solutions.

VI. MMWAVE FIELD EXPERIMENTS

We rely on our prior field experiments with mmWave waves in agricultural fields. A comprehensive discussion of the experimental methodology and results of these experiments is presented in [14], [15] along with open source data [16]. Since we focus on the scattering effect caused by canopy surfaces in this work, in the following, we mainly discuss the relevant methodology and experiments.

We focus on scattering off corn canopy because our prior results in [15] reveal that soybean canopy, due to its uniform distribution, relatively low height, and the configuration of our experiment equipment, does not result in considerable scattering. In our field experiments, a pair of TerraGragh (TG) 60-GHz channel sounders [34] with IEEE 802.11ad waveform was deployed in a research farm with outdoor agricultural fields. The radio front-end of the TG sounder has a phased antenna array consisting of 8×36 elements that form a halfpower beamwidth of 2.8° and 12° in the azimuth and elevation planes, respectively. The nominal effective isotropic radiated power (EIRP) is around 36 dBm. A complete list of parameters of the channel sounder is shown in Table I.

In the experiments, we utilize different operation modes, including an extensive beam sweeping mode (in the azimuth plane ranging from -45° to $+45^{\circ}$ with a step size of 1.4° and a live channel sounding mode that captures the channel impulse response (CIR) in real-time. During beam sweeping, a total of 4,906 beam pairs from each of the 64 distinct beams at both Tx and Rx are formed to find viable paths to establish a link [34], [35]. Accordingly, a beam pair with the maximum signal-to-noise ratio (SNR) is selected for live channel-sounding measurements.

At the corn field, which is located at the Eastern Nebraska Research, Extension and Education Center (ENREEC) Field

TABLE II: Details of related experiments with crop & measurement heights, and measurement distances.

Date	Crop height [ft]	Measurement heights [ft]	Link distances [m]	Angle of incidence [°]
July 16	6.8	10	19.2, 41.1, 61.8, 77	[84.2, 88.5]
Oct. 12	7.9	10	77	89.0
Nov. 16	1.6 (corn stubble)	10	19.2, 41.1, 61.8, 77	[75.1, 87.1]

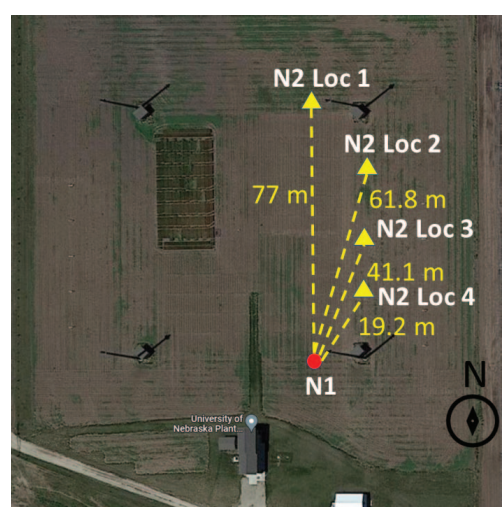


Fig. 5: Satellite images of the experimental sites (Source: Google Maps) [15].

Phenotyping Facility near Mead, Nebraska [23], we separated the transmitter (Tx) and receiver (Rx) at a maximum distance of 77 m, as shown in Fig. 5. A detailed list of experiment configurations can be found in Table II. In each of the distance and height configurations, we collected the following data to facilitate modeling the scattering effect of the corn canopy.

A. Data Collection

The TG sounder provides the received power, path loss, effective isotropic radiated power (EIRP), root-mean-square (RMS) delay spread, channel impulse response, and signal-to-noise ratio. In addition to the channel sounder, a weather station is available at the ENREEC facility, which measures weather-related metrics, such as relative humidity and temperature. The fact that the wavelength at 60 GHz (≈ 5 mm) is comparable to the size of the tip of crop leaves leads to a unique scattering environment. To this end, crop-relevant metrics are needed to facilitate quantitative analysis of the scattering effect.

B. Crop-related Metrics

The water content in crop leaves is highly correlated with growth stages [36]. Measured data shows that the corn has an average value of 72.3% volumetric water content, with a standard deviation of 2.7% during the growing season¹. The estimated water content is significantly lower in October,

TABLE III: Parameters in Simulations

Parameter	Value
Temperature	20 °C
Leaf thickness	0.2 mm
Impedance of air	377 Ω
Volumetric water content in leaves	72.3%
Water salinity	1%
Corn leaf length	25 cm

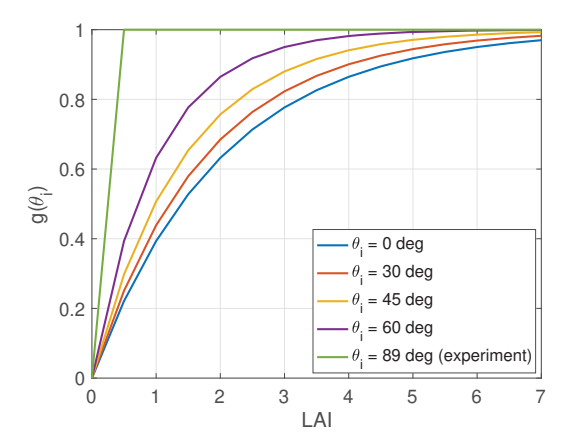


Fig. 6: Fractional vegetation cover as a function of LAI at different angles of incidence.

which can range from 22% to $32\%^2$. As crops lose water, their leaves usually become stiffer. As we discuss in Section IV, this corresponds to a drop in the dielectric constant of leaves.

VII. NUMERICAL RESULTS

We validate the model in Section IV based on simulations on the power scattered off crop canopy at different growth stages with a center frequency of 60.48 GHz. The numerical results are compared with experimental data collected from field measurements conducted from July to November 2021. A list of parameters used in our simulations is shown in Table III.

As shown in Fig. 6, the fractional vegetation cover $(g(\theta_i))$ varies with the angle of incidence and, intuitively, LAI. As LAI decreases, except at shallow grazing angles, g also decreases, exposing more soil as compared to leaves. Under different angles of incidence, the value of $g(\theta_i)$ increases as θ_i increases, mitigating the gaps between soil and leaves. The

¹https://cropwatch.unl.edu/water-management

²https://cropwatch.unl.edu/harvesting-drying-storing-late-maturing-high-moisture-corn

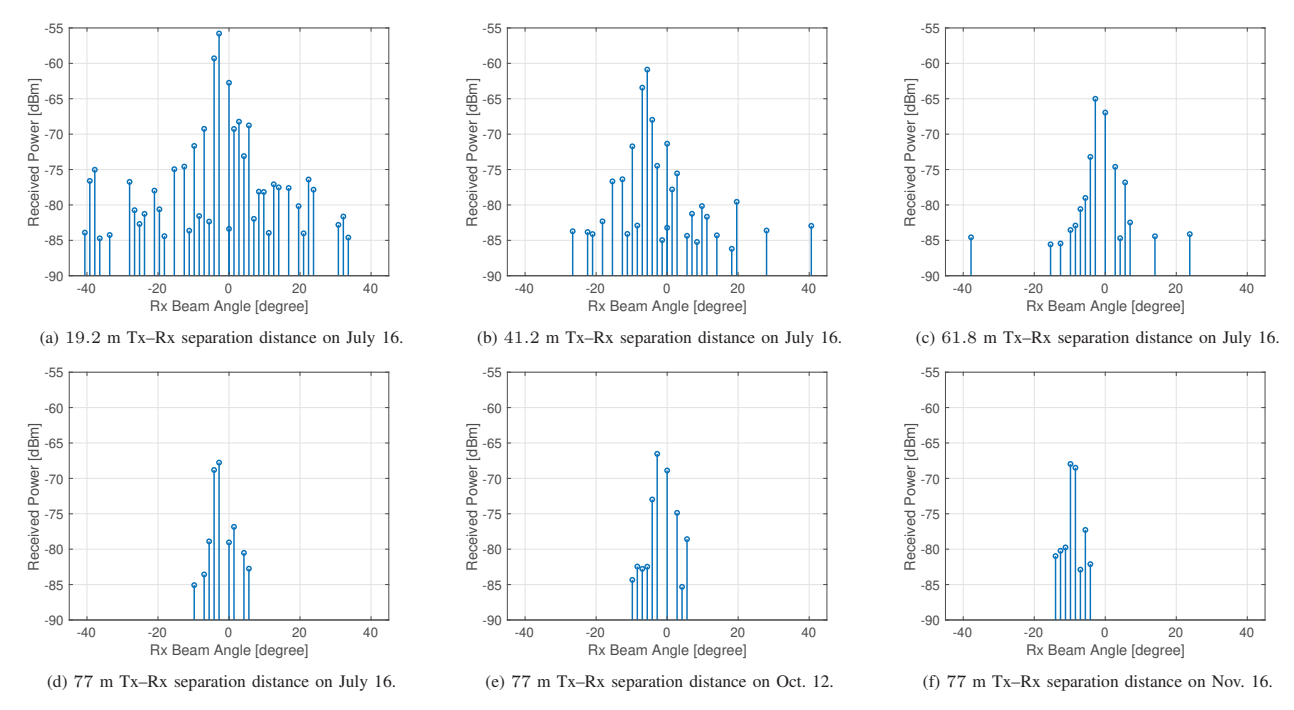


Fig. 7: Measured received signal patterns at different growth stages from July (peak growing season) to November (after harvest).

TABLE IV: Simulation Results Based on Field Experiment Configurations

θ_i	LAI	$h_{ m rms}$ [mm]	Scattering Loss [dB]
84.2°	3.5	13.0	18.7
87.3°	3.5	13.0	12.1
88.2°	3.5	13.0	8.5
88.5°	3.5	13.0	6.6
89.0°	2	10.0	1.5

permittivity of a leaf, when it is fresh in July, and temperature is $T=20\,^{\circ}C$, is calculated as 5.2769+6.3925i, which matches well with the model in [28]. As the crops mature and leaves lose water, the permittivity drops significantly, especially the imaginary part, which serves as the medium loss factor. A smaller value implies that the medium absorbs less energy and, according to the conservation of energy, more energy is scattered back into the air.

The scattering loss factor computed from (9) is shown in Table IV, where five different angles of incidence and two LAI values based on field measurement data are considered. It is shown that when the LAI is high and with an incidence angle of 84.2° , the scattering loss is calculated as 18.7 dB, which is higher compared to that when the angle of incidence increases. As LAI decreases with the maturity of crops, the scattering loss also drops. This trend is also reflected in the received power patterns in field experiment data, which are shown in Figs. 7. In Figs. 7a to 7d, the impacts of Tx–Rx separation on the received power distribution can be observed based on data collected on the same day (July 16th). The received power

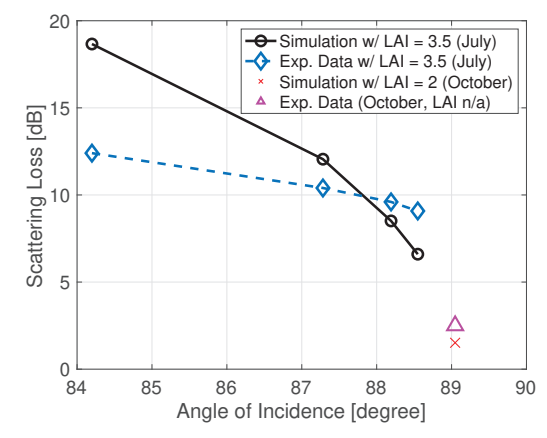


Fig. 8: Comparison of simulation and field experiment results (Note: "n/a" denotes that the value of LAI was not measured in October 2021.)

decreases as the distance increases. The paths on both sides of the main beam range (the highest two or three adjacent beams with $2.8^{\circ}-5.2^{\circ}$ angular range) indicate scattered paths. It is observed from the July 16 data that regardless of distance, the scattering loss (i.e., the power difference between the most aligned beam with the maximum received power and the scattered path) is relatively consistent with a slightly decreasing value of approximately 10 dB. Comparing the power patterns in July and October with the same configuration in Figs. 7d and 7e, a much stronger scattering path with less than 3 dB difference between the main beam and the strongest scattering

path is observed in October. In November, after the harvest season, the received signal pattern shows a narrower angular range of paths in the absence of crop canopy (Fig. 7f). The results indicate that crop canopy provides diffuse scattering with a large angular spread. This angular spread decreases as transmission distance increases.

In Fig. 8, the scattering loss is shown as a function of the angle of incidence using simulation and experimental data. It can be observed that lower LAI (estimated as around 2 in simulation for October) leads to approximately 5 dB lower scattering loss compared to higher LAI (around 3.5 in midJuly). This indicates that as crops mature and lose water (i.e., decreasing LAI), the permittivity of leaves also decreases. Therefore, more energy will be radiated back into the air. In addition, from the perspective of sensing using received signals, one could retrieve the scattering loss to classify the level of LAI based on the distinct differences.

VIII. CONCLUSION

In this work, we model mmWave signals' scattering effect due to crop canopies at the 60 GHz with agricultural metrics associated with the leaf area index. A Rayleigh roughness criterion-based approach is used to capture the scattering loss at different crop conditions. Numerical results at different angles of incidence and leaf area index values based on the developed models show a good fit with the experimental data collected from our field measurements. We demonstrate that the scattering loss decreases as the water content in the canopy decreases, which can serve as a metric for leaf area index sensing.

REFERENCES

- I. F. Akyildiz, A. Kak, and S. Nie, "6G and beyond: The future of wireless communications systems," *IEEE access*, vol. 8, pp. 133 995– 134 030, 2020.
- [2] A. Alkhateeb, O. El Ayach, G. Leus, and R. W. Heath, "Channel estimation and hybrid precoding for millimeter wave cellular systems," *IEEE journal of selected topics in signal processing*, vol. 8, no. 5, pp. 831–846, 2014.
- [3] M. Kamel, W. Hamouda, and A. Youssef, "Ultra-dense networks: A survey," *IEEE Communications Surveys and Tutorials*, vol. 18, no. 4, pp. 2522–2545, 2016.
- [4] M. C. Vuran, A. Salam, R. Wong, and S. Irmak, "Internet of underground things in precision agriculture: Architecture and technology aspects," *Ad Hoc Networks*, vol. 81, pp. 160–173, 2018.
- [5] N. Chamara, M. D. Islam, G. F. Bai, Y. Shi, and Y. Ge, "Ag-IoT for crop and environment monitoring: Past, present, and future," *Agricultural Systems*, vol. 203, p. 103497, 2022.
- [6] G. Bai and Y. Ge, "Crop Sensing and Its Application in Precision Agriculture and Crop Phenotyping," Fundamentals of Agricultural and Field Robotics, pp. 137–155, 2021.
- [7] A. Miyao, Y. Iwasaki, H. Kitano, J.-I. Itoh, M. Maekawa, K. Murata, O. Yatou, Y. Nagato, and H. Hirochika, "A large-scale collection of phenotypic data describing an insertional mutant population to facilitate functional analysis of rice genes," *Plant molecular biology*, vol. 63, pp. 625–635, 2007.
- [8] R. T. Furbank and M. Tester, "Phenomics-technologies to relieve the phenotyping bottleneck," *Trends in plant science*, vol. 16, no. 12, pp. 635–644, 2011.
- [9] A. A. Goulianos, A. L. Freire, T. Barratt, E. Mellios, P. Cain, M. Rumney, A. Nix, and M. Beach, "Measurements and characterisation of surface scattering at 60 GHz," in 2017 IEEE 86th Vehicular Technology Conference (VTC-Fall). IEEE, 2017, pp. 1–5.

- [10] S. Ju, S. H. A. Shah, M. A. Javed, J. Li, G. Palteru, J. Robin, Y. Xing, O. Kanhere, and T. S. Rappaport, "Scattering mechanisms and modeling for terahertz wireless communications," in *ICC* 2019-2019 IEEE International Conference on Communications (ICC). IEEE, 2019, pp. 1–7.
- [11] J. Ma, R. Shrestha, W. Zhang, L. Moeller, and D. M. Mittleman, "Terahertz wireless links using diffuse scattering from rough surfaces," *IEEE Transactions on Terahertz Science and Technology*, vol. 9, no. 5, pp. 463–470, 2019.
- [12] S. Bakirtzis, T. Hashimoto, and C. D. Sarris, "FDTD-based diffuse scattering and transmission models for ray tracing of millimeter-wave communication systems," *IEEE Transactions on Antennas and Propa*gation, vol. 69, no. 6, pp. 3389–3398, 2020.
- [13] F. T. Ulaby, T. Van Deventer, J. East, T. Haddock, and M. Coluzzi, "Millimeter-wave bistatic scattering from ground and vegetation targets," *IEEE Transactions on Geoscience and Remote Sensing*, vol. 26, no. 3, pp. 229–243, 1988.
- [14] M. C. Vuran, M. M. Lunar, S. Nie, Y. Ge, S. Pitla, G. Bai, and C. E. Koksal, "Millimeter-Wave Agricultural Channel Measurements in Corn and Soybean Fields at Different Growth Stages," in *IEEE International Symposium on Antennas and Propagation and USNC-URSI Radio Science Meeting*, July 2022.
- [15] S. Nie, M. M. Lunar, G. Bai, Y. Ge, S. Pitla, C. E. Koksal, and M. C. Vuran, "mmWave on a Farm: Channel Modeling for Wireless Agricultural Networks at Broadband Millimeter-Wave Frequency," in 2022 19th Annual IEEE International Conference on Sensing, Communication, and Networking (SECON), 2022, pp. 388–396.
- [16] —, "mmWave on a Farm: Channel modeling for wireless agricultural networks at broadband millimeter-wave frequency [Data file]," 2022, available from IEEE Dataport. [Online]. Available: https://dx.doi.org/10.21227/9nxq-4t62
- [17] J. Sanderson, T. Daynard, and M. Tollenaar, "A mathematical model of the shape of corn leaves," *Canadian Journal of Plant Science*, vol. 61, no. 4, pp. 1009–1011, 1981.
- [18] I. Warrington and E. Kanemasu, "Corn Growth Response to Temperature and Photoperiod II. Leaf-Initiation and Leaf-Appearance Rates 1," *Agronomy Journal*, vol. 75, no. 5, pp. 755–761, 1983.
- [19] S. Jacquemoud, C. Bacour, H. Poilve, and J.-P. Frangi, "Comparison of four radiative transfer models to simulate plant canopies reflectance: Direct and inverse mode," *Remote Sensing of Environment*, vol. 74, no. 3, pp. 471–481, 2000.
- [20] A. Nichiporovich, "Properties of plant crops as an optical system," Soviet plant physiology, vol. 8, pp. 428–435, 1961.
- [21] F. Fang, "The retrieval of leaf inclination angle and leaf area index in maize," Master's thesis, University of Twente, 2015.
- [22] M. C. Anderson, J. M. Norman, W. P. Kustas, F. Li, J. H. Prueger, and J. R. Mecikalski, "Effects of vegetation clumping on two–source model estimates of surface energy fluxes from an agricultural landscape during SMACEX," *Journal of Hydrometeorology*, vol. 6, no. 6, pp. 892–909, 2005.
- [23] G. Bai, Y. Ge, D. Scoby, B. Leavitt, V. Stoerger, N. Kirchgessner, S. Irmak, G. Graef, J. Schnable, and T. Awada, "NU-Spidercam: A largescale, cable-driven, integrated sensing and robotic system for advanced phenotyping, remote sensing, and agronomic research," *Computers and Electronics in Agriculture*, vol. 160, pp. 71–81, 2019.
- [24] N. J. Bréda, "Ground-based measurements of leaf area index: a review of methods, instruments and current controversies," *Journal of experimental* botany, vol. 54, no. 392, pp. 2403–2417, 2003.
- [25] S. Mensah, B. du Toit, and T. Seifert, "Diversity-biomass relationship across forest layers: implications for niche complementarity and selection effects," *Oecologia*, vol. 187, pp. 783–795, 2018.
- [26] C. Matzler, "Microwave (1-100 GHz) dielectric model of leaves," *IEEE Transactions on Geoscience and Remote Sensing*, vol. 32, no. 4, pp. 947–949, 1994.
- [27] D. Long and F. Ulaby, Microwave radar and radiometric remote sensing. Artech, 2015.
- [28] T. Senior, K. Sarabandi, and F. Ulaby, "Measuring and modeling the backscattering cross section of a leaf," *Radio Science*, vol. 22, no. 06, pp. 1109–1116, 1987.
- [29] P. Beckmann and A. Spizzichino, "The scattering of electromagnetic waves from rough surfaces," *Norwood*, 1987.
- [30] J. A. Peiffer, M. C. Romay, M. A. Gore, S. A. Flint-Garcia, Z. Zhang, M. J. Millard, C. A. Gardner, M. D. McMullen, J. B. Holland, P. J.

- Bradbury et al., "The genetic architecture of maize height," Genetics, vol. 196, no. 4, pp. 1337–1356, 2014.
- [31] A. K. Fung, "Microwave scattering and emission models and their applications," *Norwood, MA: Artech House, 1994.*, 1994.
- [32] N. S. Skowronski, K. L. Clark, M. Duveneck, and J. Hom, "Three-dimensional canopy fuel loading predicted using upward and downward sensing LiDAR systems," *Remote Sensing of Environment*, vol. 115, no. 2, pp. 703–714, 2011.
- [33] J. A. Zhang, F. Liu, C. Masouros, R. W. Heath, Z. Feng, L. Zheng, and A. Petropulu, "An overview of signal processing techniques for joint communication and radar sensing," *IEEE Journal of Selected Topics in Signal Processing*, vol. 15, no. 6, pp. 1295–1315, 2021.
- [34] A. Shkel, A. Mehrabani, and J. Kusuma, "A Configurable 60GHz Phased Array Platform for Multi-Link mmWave Channel Characterization," in 2021 IEEE ICC Workshops, 2021, pp. 1–6.
- [35] Telecom Infra Project, "TIP Channel Sounder Program Results Summary Report," 2020. [Online]. Available: https://telecominfraproject.com/ mmwave/
- [36] F. Olasantan, "The effects on soil temperature and moisture content and crop growth and yield of intercropping maize with melon (colocynthis vulgaris)," *Experimental Agriculture*, vol. 24, no. 1, pp. 67–74, 1988.